Low Velocity Impact Response of Reinforced Concrete Beams: Experimental and Numerical Investigation

Satadru Das Adhikary[1,*], Bing Li[2] and Kazunori Fujikake[3]
[1]Research Fellow, Department of Civil and Environmental Engineering, National University of Singapore, Singapore 117576
[2]Associate Professor, School of Civil and Environmental Engineering, Nanyang Technological University, Singapore 639798
[3]Professor, School of Civil and Environmental Engineering, National Defense Academy, Yokosuka, Japan 239 8686

Received on 14 Sept 2014; Accepted on 20 Jan 2015

ABSTRACT
In general, transition in the mode of failure from flexure failure at the static loading to shear failure at low velocity impact in reinforced concrete (RC) beams has been reported in the literature. To quantify the above-mentioned statement, a drop-weight impact test program was carried out on RC beams. The test results showed that no shear failure has been occurred under impact loading in statically flexure-critical beams (i.e., shear to bending resistance ration greater than one) however with increasing drop-heights more localized failure with extensive concrete crushing at the impact region was observed. Impact interface (i.e., direct impact or with some interface such as steel or plywood plate in between impactor and beam) could be one reason that the change in failure mode has not been observed in the current test program. To simulate the structural impact response in details, a three-dimensional nonlinear finite element (FE) model was also developed. Numerical results agreed well with the test results obtained from current test program and also from the literature. Finally, the numerical model was used to conduct parametric studies to evaluate the effects of design parameters (e.g., ratio of beam- mass to impactor-mass, longitudinal reinforcement ratio, compressive strength of concrete and boundary conditions etc.) on impact responses and failure modes.

Keywords: RC beam; Drop-weight impact loading; Impact responses; failure modes; Finite element

*Corresponding author. *Email address*: 2020satadru@gmail.com

1. INTRODUCTION

With the rapid infrastructural development around the world, a greater number of structures are naturally being exposed to various types of impact load during their service life. Reinforced concrete (RC) structures especially have been widely used over the years by engineers in the design and construction of protective structures to resist impact loads. Typical examples are direct human action (e.g., impact by people themselves when running, jumping or falling, impact of objects when dropped or in the process of being moved, impact of thrown objects); vehicle accidents (e.g., possible impact of vehicle on and along traffic route); aircraft accidents; falling and swinging objects resulting from accidents during construction; flying debris or objects generated by explosions; falling rocks on rock-sheds in mountainous regions; tornado or tsunami- borne debris impact; marine and offshore structures exposed to ship and ice impact etc. In all these cases, the impactors or projectiles vary broadly in terms of their shapes and sizes, impact velocities, hardness, rigidities, impact attitudes (i.e., obliquity, yaw, pitch, rotation, tumbling) and produce wide spectrum of response and damage to the target. An impactor or projectile can be classified into three types, i.e. hard projectile, soft projectile and jet projectile depending on relative material strength. For example, an aircraft impact fuselage hitting a concrete target can be considered as soft projectile impact while the impact of an aircraft engine may be regarded as hard projectile impact.

Impact loading represents severe loading conditions with a force of great intensity applied in a short duration. Impact loading can be categorized into two types:single point loading and distributed impact loading. When a structures strike by an impactor or striker at a particular point that is called single point impact; whereas explosions or blasts would bring about distributed impact loading. Banthia [1] summarized three distinct situations in a typical impact event by considering the size and mass of the impacting body: (i) a very large object struck by a small impacting mass, (ii) an impact involving comparable masses, (iii) a small object struck by a large impactor. Although, the third case is comparatively rare, the first and second cases are often encountered. In the first case, due to the massiveness of impacted objects, damage is mainly confined to the contact zone. In the case of comparable masses, the behavior of impacted structure is mainly governed by global effects (i.e., bending, shear and membrane responses). Whilst the third case has been investigated by numerous researchers and several empirical formulae have suggested. Normally, global response becomes important for relatively large or similar mass projectile (as compared to target) with low impact velocity while local effects become dominant for relatively small mass projectile (as compared to target) with high impact velocity.

Low velocity impact tests can be classified mainly into two categories such as drop-weight type and pendulum type, differing in the way the corresponding hammer strikes the specimen. In the case of first type, impactor having known weight is dropped on a specimen from a certain drop - height. A pendulum-type hammer is used to deliver impact for the second one by releasing the swing hammer from a certain drop-height. Conventional Charpy impact test is a standardized test which determines the amount of energy required for fracturing the specimen. Gopalaratnam et al. [2] described the modified instrumented Charpy test in evaluating the dynamic behavior of cement-based composite specimens. However, pendulum type hammer can also be used for large scale testing of structural components [3]. Furthermore, it is noted that impulsive loading on structures can also be generated by gas gun and contact blast loading. RC structures are composite constructs, constituting plain concrete and steel reinforcements. It is well known that constitutive characteristics of plain concrete and steel reinforcements are strain rate dependent. Resistance, stiffness and ductility (or brittleness) of structural members

can be affected by the loading rates. Drop-weight impact loading cannot be merely adjudged as an extreme case of high rate loading because of the involvement of severe inertia forces, energy transfer mechanism and complex pattern of stress waves. In this case, several design parameters such as mass, initial velocity of the impactor and the stiffness of the contact region affect the structural behavior. The behavior of a structural component under low velocity impact may consist of two response phases as shown in Fig. 1: the local response due to the stress wave that occurs at the impacting point immediately after impact; and the overall response including the free vibration of the whole structural member [4]. As the structural members behave differently under impact as compared to static loading, it is important to attain a better understanding of the performance and vulnerability of RC structures under impact loading so as to mitigate the catastrophic failure.

This paper is devoted on the assessment of the structural response of RC beams subjected to low velocity impact (<10 m/s) at its midspan. Much research [5-12] has been conducted on evaluating the impact response of RC beams; however little effort has been made towards determining the impact responses of beams by considering several parameters. Thus, drop-weight impact test was performed for various heights on beams by varying span length, cross-sections, shear span to effective depth ratios (where shear span is the half of the effective span length of beam and effective depth is the distance from the top surface of beam to centre of tensile reinforcements), longitudinal and transverse reinforcement ratios and static shear to bending resistance ratio. Another objective is to examine the failure modes of beams as this is reported in literature that shear failure occurs in RC beams under impact

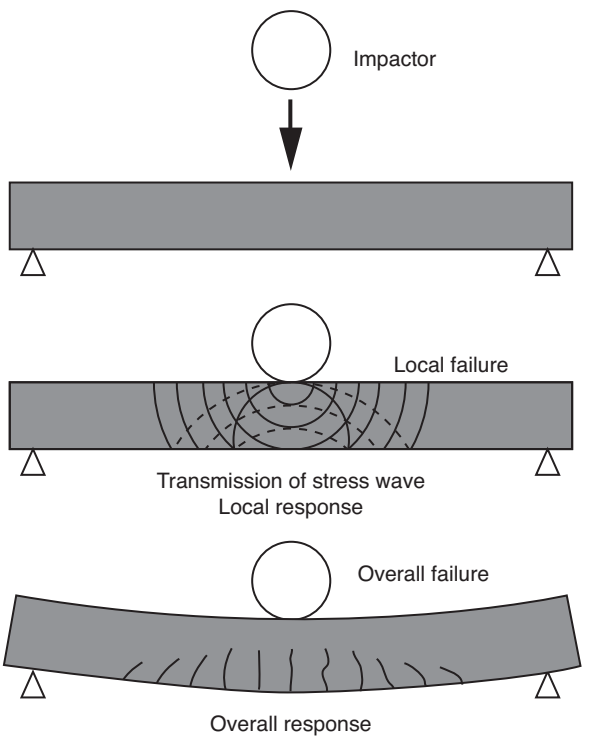

Figure 1. Impact responses of a RC member (4)

loading while same specimens failed in flexure under static loadings [13, 14]. Moreover, a three dimensional nonlinear finite element (FE) model is developed to validate the test results from current test program and the test results from the literature and then the numerical model is employed further to conduct parametric studies. The effects of various parameters on the behavior and failure mode of RC beam under various drop-heights have been investigated.

2. EXPERIMENTAL OVERVIEW

The experimental program carried out in two phases: drop-weight impact tests and static tests (Fig. 2). The impact test program consisting 30 RC beams were divided into two groups in terms of their shear span-to-effective depth ratios (a/d -3.3, 3.8 and 5.7). Each group had three types of specimens distinguished by their shear reinforcement ratios. Each 3.3 series had 4 identical specimens whereas 3.8 and 5.7 series had 3 identical specimens. Table 1 presents the overview of the entire test program including the considered drop-heights. Mass ratios (α) i.e., ratios of the mass of the beams (m_b) to the impactor-mass (m_i) for a/d -3.3, 3.8

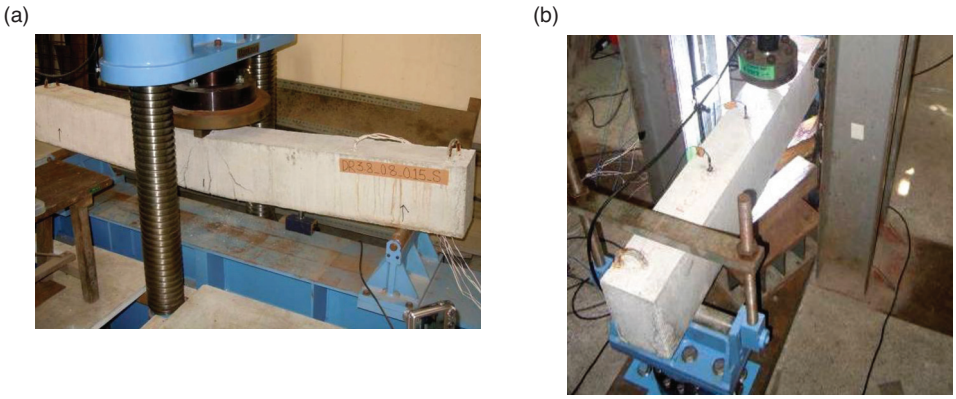

Figure 2. Test set up (a) Static; (b) Drop-weight impact

Table 1. Test program

Beam designation	Static test	Drop height (m)	Impact velocity (m/s)	Impact energy (kJ)
DR3.3_2.4		0.15, 0.30, 0.60, 1.2	1.72, 2.43, 3.43, 4.85	0.44, 0.88, 1.77, 3.53
DR3.3_2.4_0.12	*	0.30, 0.60, 0.90, 1.2	2.43, 3.43, 4.20, 4.85	0.88, 1.77, 2.65, 3.53
DR3.3_2.4_0.56		0.60, 0.90, 1.2, 1.6	3.43, 4.20, 4.85, 5.60	1.77, 2.65, 3.53, 4.71
SR3.8_0.8		0.30, 0.60, 0.90	2.43, 3.43, 4.20	0.88, 1.77, 2.65
DR3.8_0.8_0.11	√	0.60, 0.90, 1.2	3.43, 4.20, 4.85	1.77, 2.65, 3.53
DR3.8_0.8_0.15		0.60, 0.90, 1.2	3.43, 4.20, 4.85	1.77, 2.65, 3.53
SR5.7_1.6		0.30, 0.45, 0.60	2.43, 2.97, 3.43	0.88, 1.32, 1.77
DR5.7_1.6_0.15	√	0.30, 0.45, 0.60	2.43, 2.97, 3.43	0.88, 1.32, 1.77
DR5.7_1.6_0.20		0.30, 0.45, 0.60	2.43, 2.97, 3.43	0.88, 1.32, 1.77

Note: √= Tested; *= FEM determined

and 5.7 specimens were 0.42, 0.49 and 0.26 respectively. The specimen denoted by SR5.7_1.6 corresponds to 'singly- reinforced' beam (SR) followed by the shear span-to effective depth ratio and percentage of longitudinal tensile reinforcement ratios. Again, DR5.7_1.6_0.20 refers to 'doubly-reinforced' beam (DR) followed by the shear span-to effective depth ratio, percentage of longitudinal tensile and compressive reinforcement ratio and percentage of shear reinforcement ratio. For impact loading, a drop-weight impact loading machine was used in which a drop-weight with a mass of 300 kg was dropped freely onto the top surface of the beam at midspan from different heights. For 3.3 series four and for 3.8 and 5.7 series specimens three different drop heights were considered. The striking head of impactor had a hemispherical tip with a radius of 90 mm. Specially designed support devices were mounted over the clear span of the beam, allowing it to rotate freely while preventing the uplift of beam during impact loading.

All beams have rectangular cross section 120 to 160 mm in width, 170 to 250 mm in depth. Beams of 3.3 series were supported over the clear span of 1400 mm whereas specimens from 3.8 and 5.7 series were supported over the clear span of 1600 mm. The longitudinal tensile reinforcement ratios are in the range of 0.8 to 2.4%. For DR beam section equal amount of reinforcements were provided in compression side. When the longitudinal tensile reinforcement ratios were calculated in terms of balanced reinforcement ratios (i.e., the reinforcement ratio at which the yielding of tensile steel and the crushing of concrete occur simultaneously), these values would be around 0.83 ρ_b, 0.28 ρ_b and 0.55 ρ_b for 3.3, 3.8 and 5.7 series respectively; where ρ_b refers to balanced reinforcement ratio in percentage. The layout of the longitudinal reinforcements, spacing of shear reinforcements and the measuring points (accelerometers for measuring accelerations and strain gauges for measuring strain of steel reinforcing bars) are shown in Fig. 3.

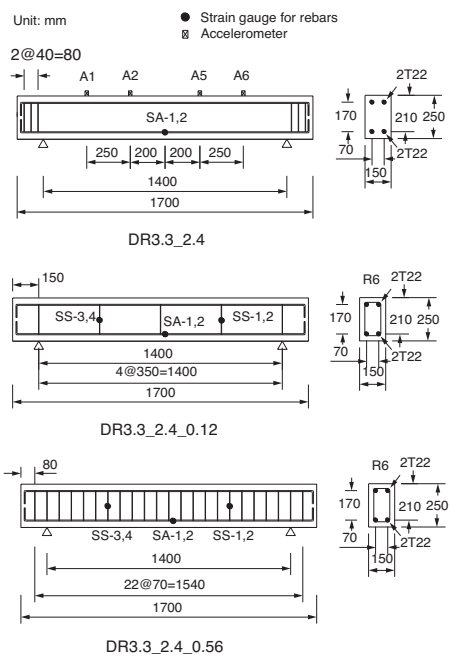

(Continued)

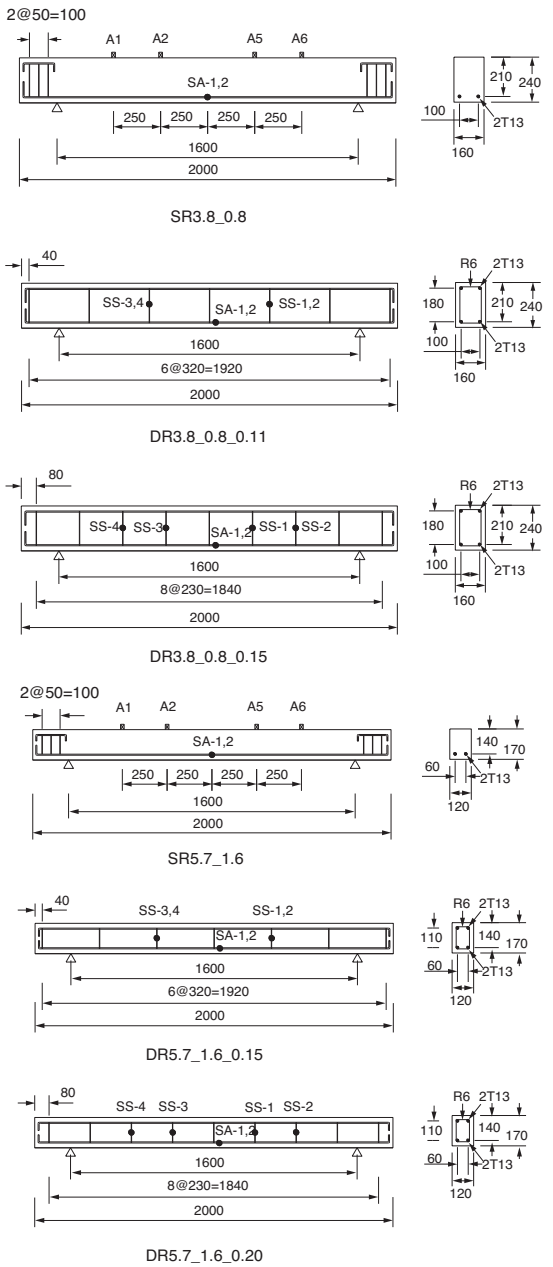

Figure 3. Dimensions of RC beams, layout of reinforcements, location of strain gauges and accelerometers

Here, 'SA' refers to the strain gauges attached at the midspan of longitudinal tensile reinforcements whereas 'SS' refers to the strain gauges attached to transverse reinforcements and A1, A2, A5 and A6 refers to the accelerometers. Longitudinal reinforcements consisted of deformed steel bars of T22 (dia.-22mm), T13 (dia.-13mm) and T13 (dia.-13mm) for *a*/*d* -3.3, 3.8 and 5.7 series specimen respectively while R6 (dia.-6mm) plain round bars were

used as transverse reinforcements for all specimens. Target concrete compressive strength at 28 days was 40 MPa with maximum aggregate size of 10 mm for all specimens. The yield strengths of T22, T13 and R6 were 520, 520 and 310 MPa respectively. All specimens were cast at the same time using ready mix concrete of same batch; thence, all specimens had an identical concrete strength. The compressive strength at 28 days obtained from three concrete cylinders was 39.0, 37.6 and 38.8 MPa respectively. The specimen details, theoretical static capacities, static expected and observed failure modes are listed in Table 2, where the static flexural and shear resistances are calculated according to ACI 318-08 [15]. To construct the specimens, steel formwork was used. Before the placement of reinforcing cages, oiling was carried out on the inside surfaces of formwork so that specimens can be removed easily and the surface of the specimens would not damage. Before the casting, concrete spacer blocks were placed in the underside as well as the side faces of transverse reinforcements to achieve clear concrete cover. Lifting hooks were mounted on both sides of the specimens to facilitate lifting process during testing. Fig. 4 shows the photos of the casting of beams and the preparation of concrete cylinders (150mm × 300 mm). After casting, damp hessian fabrics

Table 2. Details of specimens and static design parameters

Designation	Shear span to effective depth ratio	Longitudinal reinforcement ratio (%)	Transverse reinforcement ratio (%)	Bending resistance (kN)	Shear resistance (kN)	Shear to bending resistance ratio
DR3.3_2.4	3.3	2.4	0	203.7	66.2	0.33
DR3.3_2.4_0.12			0.12		87.1	0.43
DR3.3_2.4_0.56			0.56		170.4	0.84
SR3.8_0.8	3.8	0.8	0	67.83	70.45	1.04
DR3.8_0.8_0.11			0.11		67.83	93.32	1.38
DR3.8_0.8_0.15			0.15		102.3	1.51
SR5.7_1.6	5.7	1.6	0	42.4	35.32	0.83
DR5.7_1.6_0.15			0.15		50.52	1.19
DR5.7_1.6_0.20			0.20		56.4	1.33

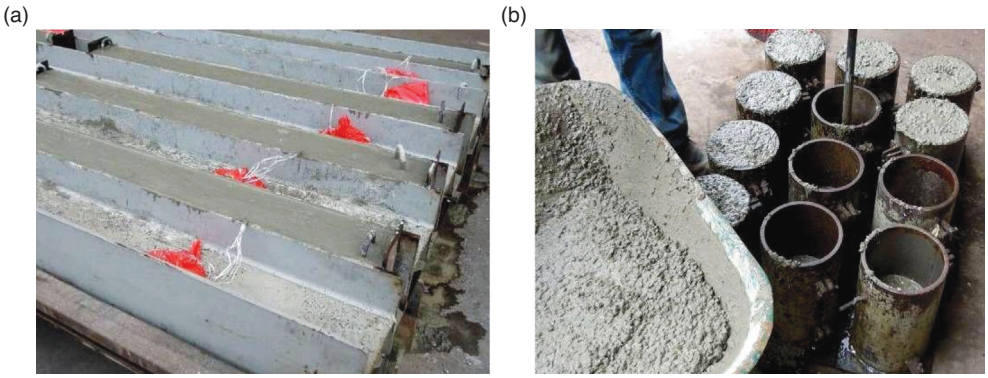

Figure 4. (a) Casting of beams; (b) preparation of concrete cylinders

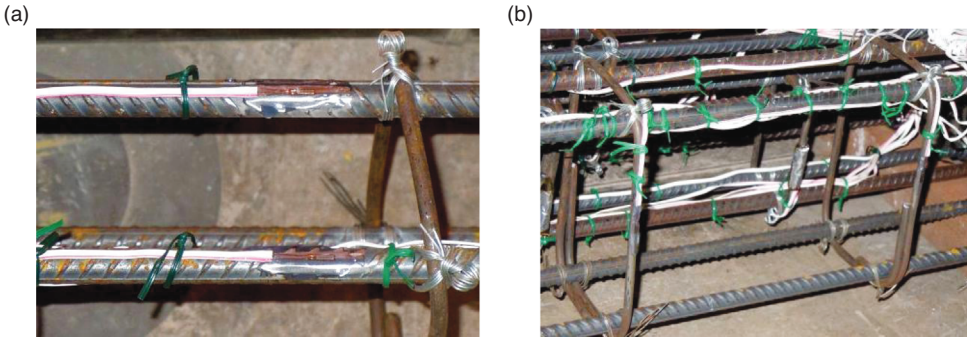

Figure 5. (a) Strain gauging in tensile longitudinal reinforcements; (b) Strain gauging in transverse reinforcements

were employed to cure the specimens for two weeks. All specimens were well instrumented to capture the loads, displacements, accelerations and the strains of steel reinforcements. The instrumentation for this test program included a load cell, strain gauges and accelerometers. Strain gauges with 3 mm gauge length were installed in the mid-span of the longitudinal tensile reinforcements and in the mid-point of the two legs of the shear reinforcements to measure the local strain. These are general purpose foil strain gauges (KFG types) with resistance of 120 Ω, maximum strain limit of 5% and linear expansion coefficient of $11 \times 10\text{-}6/^{\circ} C$. Soldering to the terminal of the gauges was not required due to the pre-attachment of three parallel vinyl-coated lead wires having length of 10 m. Before the installation of strain gauges at the specific locations, the reinforcement surfaces were grinded lightly and cleaned with alkaline and acidic chemicals. Fig. 5 shows the photos of the glued strain gauges in longitudinal tensile and transverse reinforcements. Although in Fig. 5, the strain gauge is shown in top face of the tensile reinforcements however, the reinforcement cages were inverted during the placement into the moulds; then the gauges would be in the bottom face of the tensile reinforcements. The impact load developed between the impactor and beams was measured by a dynamic load cell (frequency response 5 kHz), which was rigidly attached to the drop-weight. Four accelerometers (capacity of 1000 times gravity and resonance frequency greater than 70 kHz) were mounted on the specimens for each test (except for static loading) to measure the accelerations. The midspan deflection of RC beams was measured by laser-type variable displacement transducers (LVDTs) which have a measuring range of 80 mm. Data from the sensors were collected by a computer - based data acquisition system which has a sampling rate of 100 kHz. For getting insights about the cracking patterns and failure modes of beams, digital photography and high-speed video recording systems were employed.

3. EXPERIMENTAL RESULTS AND DISCUSSIONS

3.1. STATIC TEST RESULTS

Load vs. midspan deflection responses obtained from static tests are presented in Fig. 6 and simultaneously failure patterns are depicted in Fig 7. SR beam of 3.8 series failed in shear-critical mode with the formation of diagonal shear crack. Sharp fall of the post-peak branch in the load vs. midspan deflection curves of SR3.8_0.8 is clearly seen whereas, DR beams from same series exhibited ductile failure response. For specimens of 5.7 series, ductile

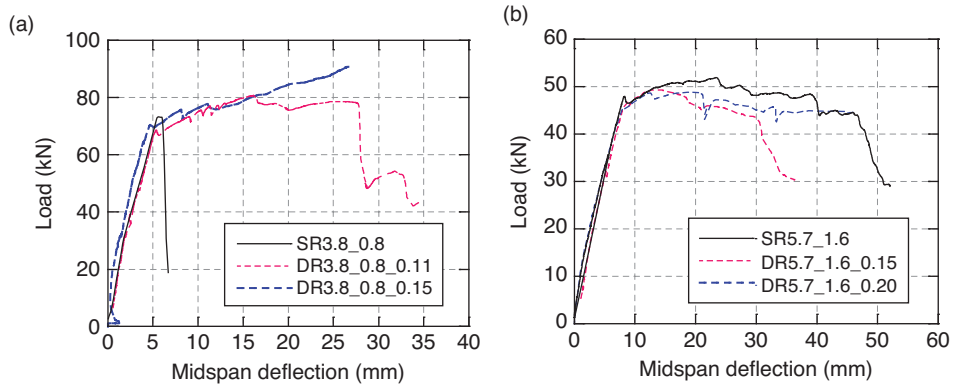

Figure 6. Static load vs. midspan responses of beams (a) 3.8 series; (b) 5.7 series

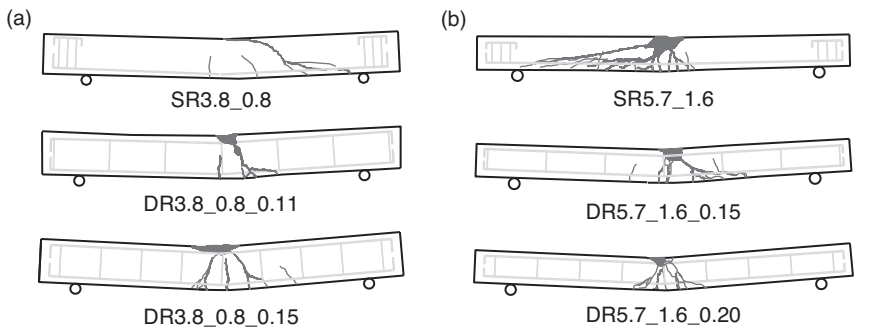

Figure 7. Failure pattern of beams under static loading (a) 3.8 series; (b) 5.7 series

failures were observed. From the picture of the crack pattern of SR5.7_1.6 diagonal crack was perceived, however this crack was formed at the ending time of the testing process or at a large deflection.

3.2. IMPACT TEST RESULTS

This section summarizes the test results obtained from the drop-weight impact tests. Time histories of midspan deflection, strain rates in longitudinal tensile reinforcements and crack patterns are summarized.

3.2.1. Time histories of midspan deflection

Fig. 8 shows the time histories of midspan deflection of beam having duration of 150 milliseconds from the beginning of impact. From these figures, it is observed that the shapes of the time histories of midspan deflection are similar of the same series specimens. Maximum and residual midspan deflection of the beam in the same series increased with the increment of the drop heights as shown in Table 3. DR3.3_2.4 specimens after reaching the peak displacements exhibited almost constant response without any vibration. DR

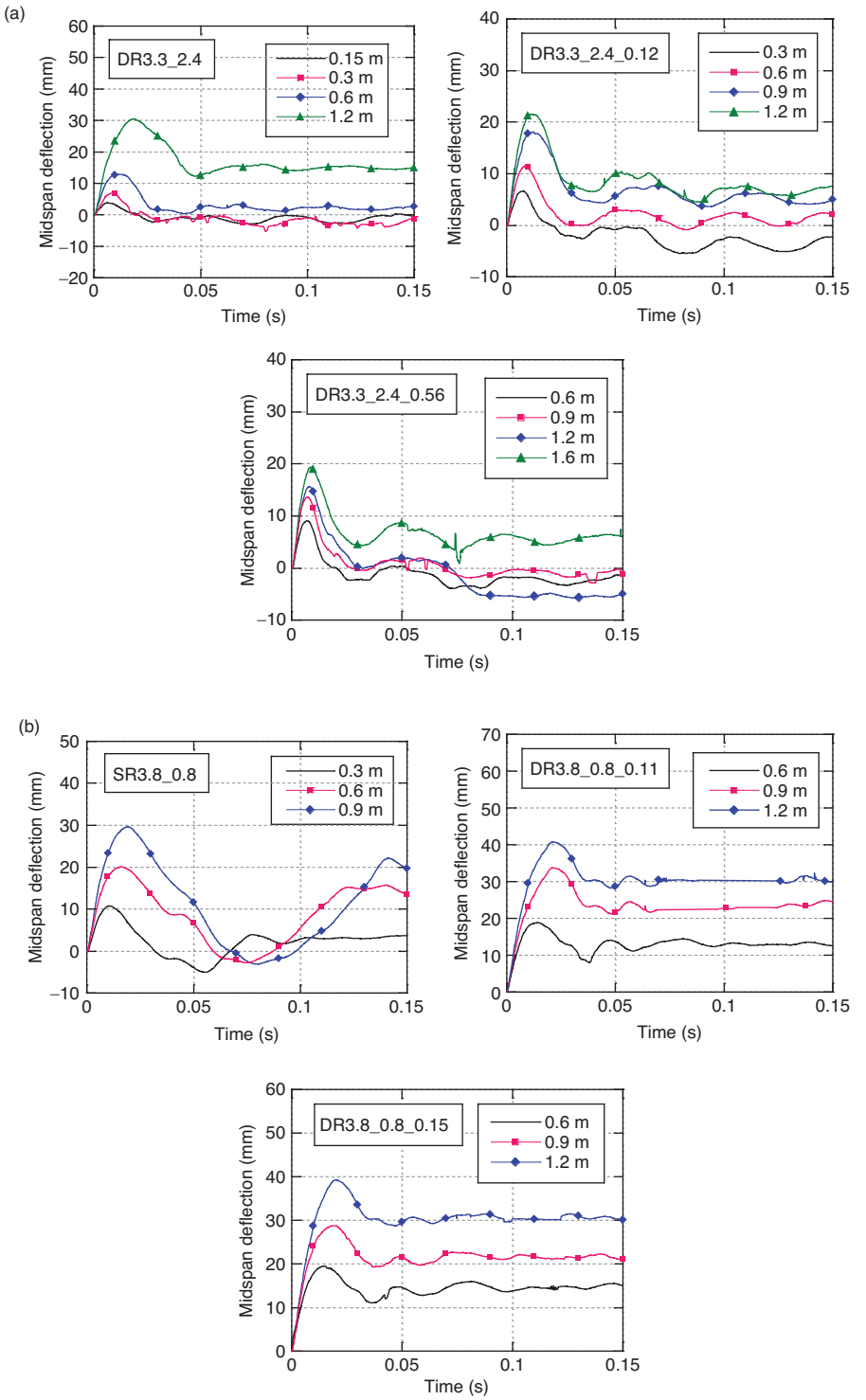
(a)
DR3.3_2.4
0.15 m
0.3 m
0.6 m
1.2 m
Midspan deflection (mm)
Time (s)
DR3.3_2.4_0.12
0.3 m
0.6 m
0.9 m
1.2 m
DR3.3_2.4_0.56
0.6 m
0.9 m
1.2 m
1.6 m
(b)
SR3.8_0.8
0.3 m
0.6 m
0.9 m
DR3.8_0.8_0.11
0.6 m
0.9 m
1.2 m
DR3.8_0.8_0.15
0.6 m
0.9 m
1.2 m

(Continued)

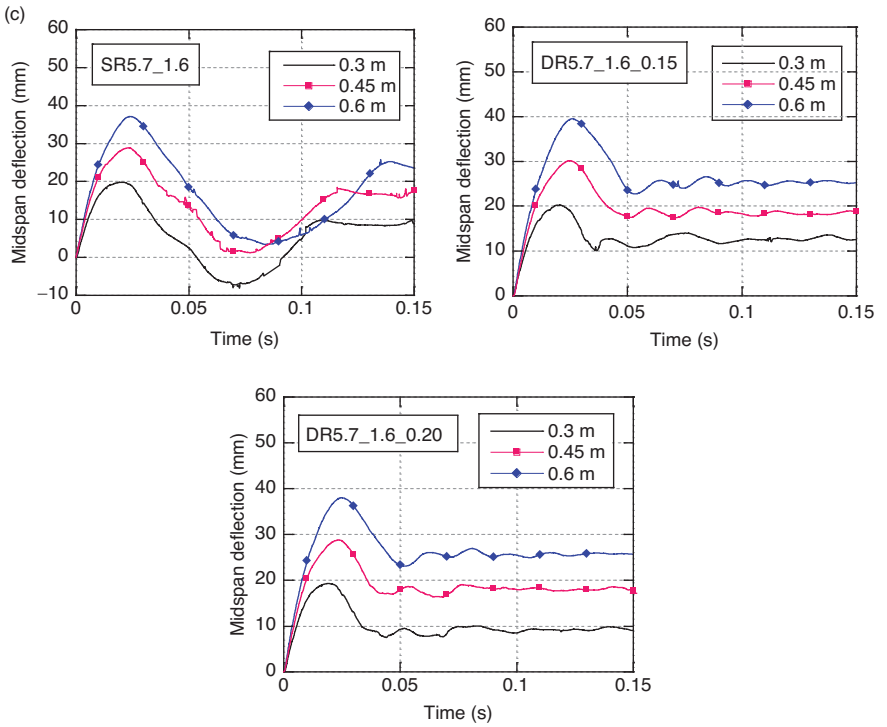

Figure 8. Time histories of midspan deflection (a) 3.3 series; (b) 3.8 series; (c) 5.7 series

3.3_2.4_0.12 and DR 3.3_2.4_0.56 almost exhibited similar response; however some vibration with small amplitude was observed in the unloading phase. For 3.8 and 5.7 series, the midspan deflection history of singly reinforced beams varied in a sinusoidal way where as for doubly reinforced beams, the initial response exhibited a half-sine wave with small amplitude vibration in unloading stage.

3.2.2. Strain rates

Effect of strain rate on material behavior (concrete and reinforcing steel) has been well documented in the literature [16-18]. Constitutive material properties for structural materials are dependent of loading rates. Impact loads introduce considerably higher strain rate as compared to static loading, resulting in different behavior in concrete and steel. Hence, it is worthwhile to determine the maximum strain rate and their variation for various drop heights considered in this test program. It was mentioned earlier that strain gauges were mounted in all longitudinal tensile reinforcements and some transverse reinforcements; however, no initiative was taken to measure the strain in concrete. Strain rates are determined from the strain-history data provided by the strain gauges. One specimen for a particular drop height is taken from each series (i.e. 3.3, 3.8 and 5.7) to present their strain rate-history data for longitudinal tensile reinforcements and transverse reinforcements. Maximum strain rates in longitudinal tensile reinforcements are found to be around 2.5, 6 and 5.9 s^{-1} for

Table 3. Maximum and residual midspan deflection of beam

Specimens	Drop heights (m)	Impact velocity (m/s)	Maximum midspan deflection (mm)	Residual midspan deflection (mm)
DR3.3_2.4	0.15	1.72	3.8	0
	0.30	2.43	6.9	0
	0.60	3.43	12.7	2.2
	1.20	4.85	30	15
DR3.3_2.4_0.12	0.30	2.43	6.4	0
	0.60	3.43	11.5	2.5
	0.90	4.20	18.2	5
	1.20	4.85	21.6	7.8
DR3.3_2.4_0.56	0.60	3.43	9.0	0
	0.90	4.20	13.4	0
	1.20	4.85	15.7	0
	1.60	5.60	19.2	7.1
SR3.8_0.8	0.30	2.43	10.8	2
	0.60	3.43	20.2	12.2
	0.90	4.20	29.5	20
DR3.8_0.8_0.11	0.60	3.43	18.6	12
	0.90	4.20	34.5	23
	1.20	4.85	41.0	30
DR3.8_0.8_0.15	0.60	3.43	19.6	15
	0.90	4.20	28.8	21.2
	1.20	4.85	39.2	30.4
SR5.7_1.6	0.30	2.43	20.0	9.9
	0.45	2.97	28.8	19.1
	0.60	3.43	37.1	22.2
DR5.7_1.6_0.15	0.30	2.43	20.0	12.6
	0.45	2.97	30.0	19.6
	0.60	3.43	39.1	26.4
DR5.7_1.6_0.20	0.30	2.43	19.1	9.9
	0.45	2.97	28.8	18.4
	0.60	3.43	37.9	26.7

DR3.3_2.4_0.56, DR3.8_0.8_0.15 and DR5.7_1.6_0.15, respectively for the corresponding drop heights mentioned in Fig. 9. In general, maximum strain rates of longitudinal tensile reinforcements vary in between 1 to 7 s^{-1} for the corresponding considered drop heights of 0.15 to 1.2 m (i.e. impact velocity varies from 1.72 to 4.85 m/s).

3.2.3. Crack pattern

Besides, data collected by the sensors, the cracks developed after each test was marked and the crack widths were measured manually by crack width gauge. The widths of the diagonal crack were measured at mid-height whereas for the case of flexural cracks, measurement was taken at the bottom surface of beam at midspan. Fig. 10 shows the sketched cracks profiles of beams at each drop height. This was observed that the crack patterns and the failure modes

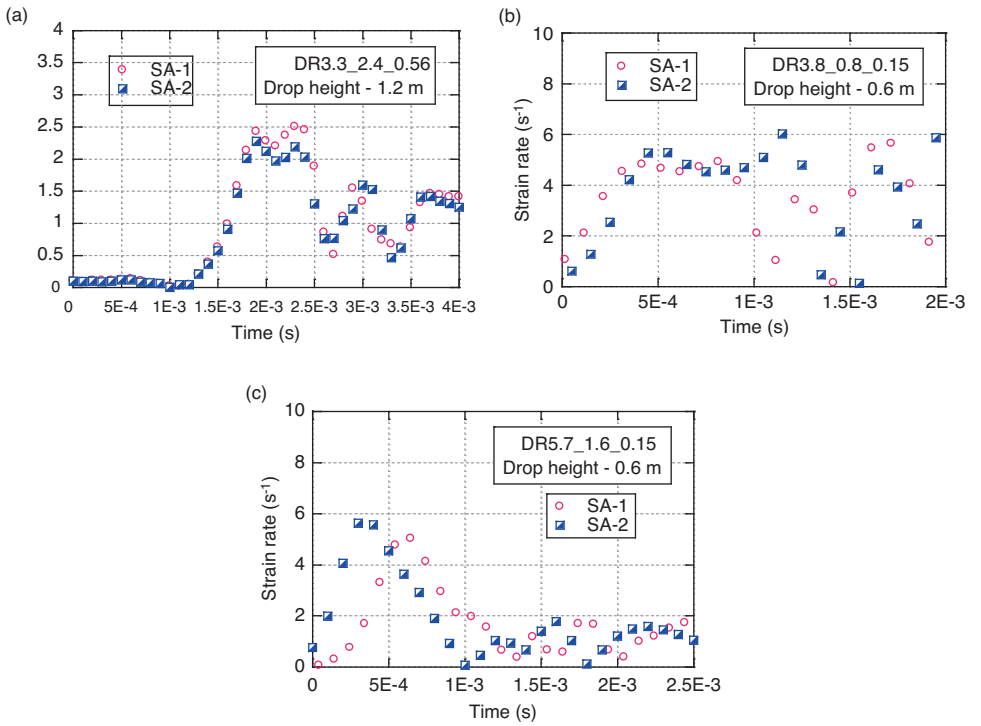

Figure 9. Variation of strain rates in longitudinal tensile reinforcements

varied between the specimens depending on their static bending and shears resistance. Detailed description of cracks profiles of beam at each drop height is summarized here: For DR3.3_2.4, no damage was observed in this beam at a drop height of 0.15 m. At 0.30 m drop height, a 0.75 mm diagonal crack was observed in the right hand side whereas another hairline diagonal crack appeared in other side. Local failure did not happen at or around the impact region. With the increment of the drop height to 0.60 m, two diagonal cracks formed in the right hand side having width of 0.65 and 1.2 mm, respectively. In the other side, hairline diagonal crack was perceived. Massive crushing and spalling of concrete occurred at the impact region. At 1.2 m drop height, the specimen suffered extensive damage with significant spalling of concrete at top, bottom and side surface of the beam in one side, exposing the longitudinal tensile and compressive bars. In the other side, spalling of concrete occurred at top and side surface of the specimen. The damage was so catastrophe that the beam was disintegrated into two components. For DR3.3_2.4_0.12, two hairline diagonal cracks were observed in this beam at a drop height of 0.30 m. At 0.60 m drop height, the diagonal cracks in one side widened, reaching up to 1 mm. Moreover, diagonal cracks forming a shear-plug (crack width 1.3 mm in one side) under the impact point were observed. With the further increment of the drop height to 0.90 m, the diagonal cracks in one side widened significantly, reaching up to 6.5 mm and in the other side, diagonal crack formed with 1.2 mm width. Like previous case, shear - plug developed at the impact point. Furthermore, local failure in terms of crushing and spalling of concrete at the impact region occurred. At 1.2 m drop height, diagonal cracks in both sides broadened extensively, attaining up to 12.5 and 4.5 mm, respectively. The local damage was quite extensive with crushing and spalling of concrete.

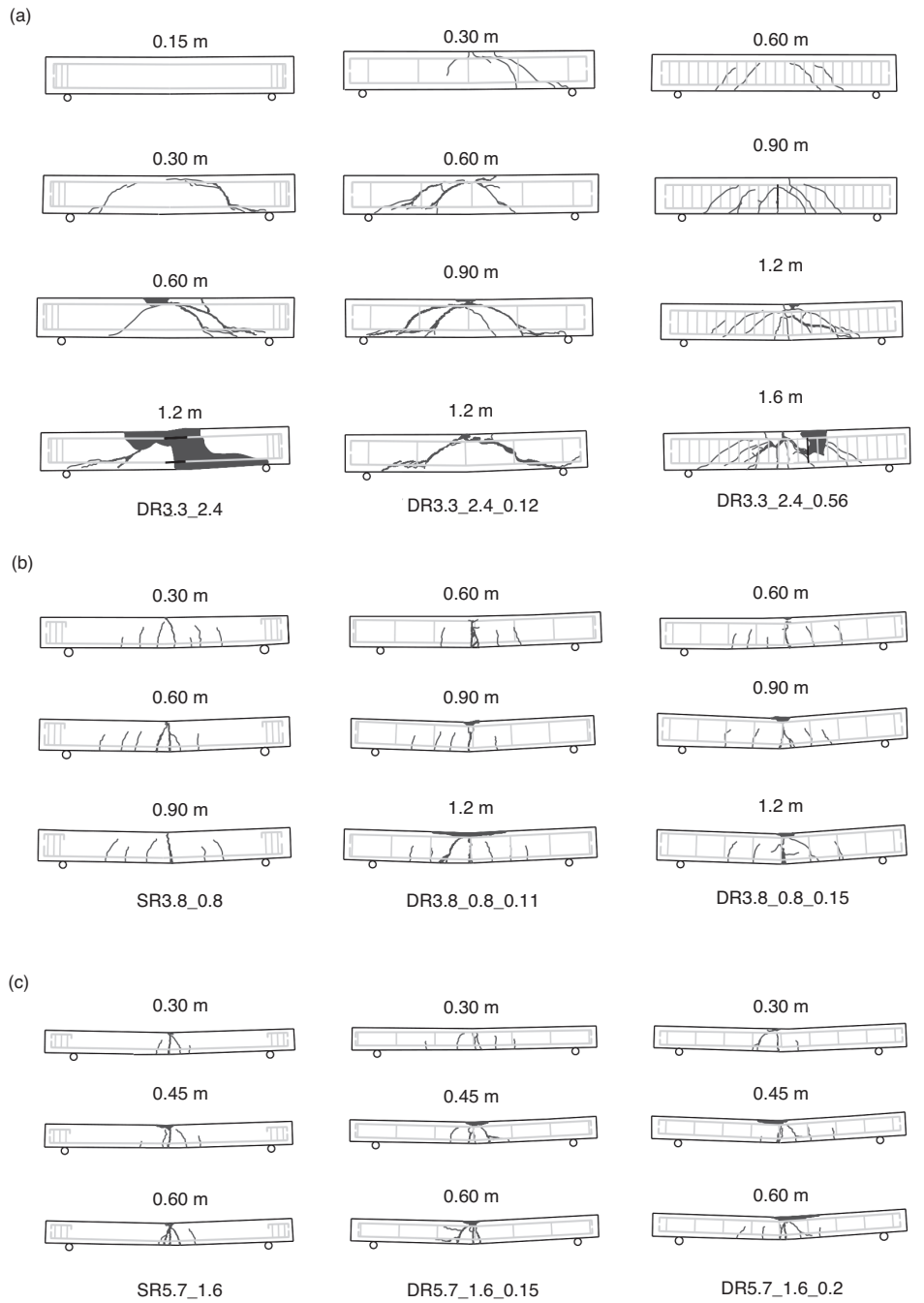

Figure 10. Crack pattern of beams (a) 3.3 series; (b) 3.8 series; (c) 5.7 series

Moreover, few horizontal cracks propagated in the longitudinal direction of beam from the impact point. For DR3.3_2.4_0.56, Hairline flexure- shear cracks were observed in this beam at a drop height of 0.60 m without any local damage. At 0.90 m drop height, the number of flexure-shear cracks increased and flexural cracks at midspan developed. Still, at this drop height, no damage in the impact region occurred. With the further increment of the drop height to 1.2 m, the flexure-shear cracks became much flatter as compared to previous two cases. Moreover, some local damage has been occurred in the impact region. Some splitting cracks were identified in the side cover of the beam. At 1.6 m drop height, the severity of damage increased significantly mainly at or around impact region, with crushing and spalling of concrete and number of flexure-shear cracks also increased. For SR3.8_0.8, typical flexure failure was observed in this beam for a drop height of 0.30 m. Flexural cracks developed from the bottom surface and propagated towards top surface of the beam. Flexural cracks (crack width 0.5 mm) underneath the impact point formed at the bottom surface and propagated towards top surface and finally crushed the compression concrete. Like previous case, almost similar type of crack pattern has been perceived at a drop height of 0.60 m. However, flexural cracks underneath the impact point widened further, reaching up to 1.4 mm. With the further increment of the drop height to 0.90 m, no too much difference in the crack pattern has been observed. However, flexural crack underneath the impact point became wider, reaching up to 1.7 mm. Moreover, local failure occurred at the impact region which combined with the flexural crack underneath the impact point disintegrated beam into two parts. For DR3.8_0.8_0.11, typical flexure failure was observed in this beam for a drop height of 0.60 m. Flexural cracks (width 5 mm) underneath the impact point developed from the bottom surface and propagated towards top surface. Moreover, some hairline flexure crack was perceived near surrounded region of midspan. At 0.9 m drop height, flexural cracks underneath the impact point became widened, attaining up to 9 mm width and successively some crushing at the impact region was noticed. With the further increment of the drop height to 1.2 m, flexure crack (width around 15 mm) was observed and massive local damage occurred at or around the impact region. For DR3.8_0.8_0.15, typical flexure failure was observed in this beam for a drop height of 0.60 m. Flexural cracks (width 1.1 mm) underneath the impact point developed from the bottom surface and propagated towards top surface. Moreover, few hairline cracks were perceived in the surrounding region. Flexural cracks underneath the impact point became widened at 0.9 m drop height. The crack almost attained 9 mm in width at bottom surface of beam. At the same time some cracking and crushing of concrete at impact region were noticed. With the further increment of the drop height to 1.2 m, flexural cracks underneath the impact point became widened significantly, reaching up to 30 mm in width. Moreover, there was significant damage occurred at the impact region. For SR 5.7_1.6, typical flexure failure was observed in this beam for a drop height of 0.30 m. Flexural cracks (crack width 1.4 mm) underneath the impact point formed at the bottom surface and propagated towards top surface and connected to the crushed and spalled concrete at the impact point. Like previous case, almost similar type of crack pattern has been perceived at a drop height of 0.45 m. However, flexural crack underneath the impact point widened more; reaching up to 6 mm. Crushing and spalling of concrete at the impact region were also noticed. These crushed and spalled concrete combined with the flexure crack crumbled the beam into two parts. With the further increment of the drop height to 0.60 m, more flexural cracks developed and the flexure cracks beneath the impact point became more broaden, reaching up to 7 mm. This crack propagated vertically upwards and disintegrated the beam into two parts. For DR5.7_1.6_0.15, Typical flexure failure was observed in this beam for a drop height of 0.30 m. Flexural cracks (crack width 1.1 mm) underneath the impact point

formed at the bottom surface and propagated towards top surface. Flexure cracks (width 5 mm) at the midspan and crushing of concrete at the impact region were perceived at drop height of 0.45 m. With the increment of the drop height to 0.60 m, both flexure crack (width 4 mm) and shear-plug were observed. Significant crushing of concrete at the impact region has also been occurred. For DR5.7_1.6_0.20, Typical flexure failure was observed in this beam for a drop height of 0.30 m. Flexural cracks (crack width 0.5 mm) underneath the impact point formed at the bottom surface and propagated towards top surface. Flexural cracks underneath the impact point widened more as compared to previous case, reaching up to 6 mm and some hairline flexure cracks were observed in the surrounded region. Moreover, some crushing and spalling of concrete at impact region were noticed. Flexural cracks underneath the impact point widened more as compared to previous case, reaching up to 6 mm and some hairline flexure cracks were observed in the surrounded region. Moreover, some crushing and spalling of concrete at impact region were noticed. The test results showed that no shear failure has been occurred under impact loading in statically flexure-critical beams (i.e., shear to bending resistance ration greater than one) however with increasing drop-heights more localized failure with extensive concrete crushing at the impact region was observed. On the contrary, transition in the mode of failure from flexure failure at the static loading to shear failure at low velocity impact in reinforced concrete (RC) beams has been reported in the literature. Impact interface (i.e., direct impact or with some interface such as steel or plywood plate in between impactor and beam) could be one reason that the change in failure mode has not been observed in the current test program. Harder and stiffer contact zone (i.e., when steel plate is placed in between the impactor and beam) produces more inertia forces (i.e., majority of impact energy transfer to beam through steel plate which accelerates the beam in the direction of impact force generating more inertia force) which assist beam failing in shear under impact loading. However, in this current test program, due to the direct contact of impactor with the beam during the impact event, majority of impact energy has been dissipated during localized crushing of concrete in the impact region. Thus, developing less inertia force due to less energy transfer to the entire span of the beam.

4. FINITE ELEMENT (FE) MODEL

The nonlinear explicit FE program LS-DYNA [19] was employed in the numerical simulation. The advantage of using explicit method is that there is no need to calculate stiffness and mass matrices for the entire system. However, explicit methods are conditionally stable and thus small time step would be needed. To make the computation stable, the selection of time step should be such that it is less than the time required for a stress wave to travel through the shortest element of a FE model. Hence, when the level of discretization increases excessive computational time would be obvious consequences. The description of modeling includes structural geometry of beam, loading plate, support roller, boundary conditions, application of loads, and relevant material properties is successively presented.

4.1. STRUCTURAL CONFIGURATION

To replicate the same experimental conditions, efforts are devoted here to develop a FE model as close to the physical system as possible. Therefore, a three-dimensional model is the obvious option to adopt. Fig. 11 shows the three-dimensional FE model of beams (i.e. one type from each series). Eight node solid hexahedron elements with a single integration point were used to represent beams (concrete), support rollers, inverted triangular plates and impactor while beam elements (2-node Hughes-Liu beam element formulation with 2 × 2

Gauss quadrature integration) were used to model steel reinforcing bars. Viscous hourglass control was used in concrete elements to avert the occurrence of hourglass modes. Stiffness-based hourglass was not used as it may cause overly stiff response even with a reduced hourglass coefficient. The FE model of the impactor divided into three sections to reproduce the same used in the experiments. First section consists of hemispherical striking head having 90 mm radius whereas solid cylinder and rectangular block were used to model the remaining part. Different mesh sizes have been considered to study mesh sensitivity during the initial stage of numerical study. Here, a mesh size of 15 mm was used to create the solid elements which seemed to be ideal as further decrease in mesh size almost generated the same results however augmented the computational time. Table 4 presents total number of elements and nodes for each beam model. The beams were supported on two cylinders made of solid elements and to prevent the uplifting of the beam after impact loading two inverted triangular plates were modeled at the top of the beam at support positions. The mesh discretization was established in such a way that the reinforcement nodes coincided with the

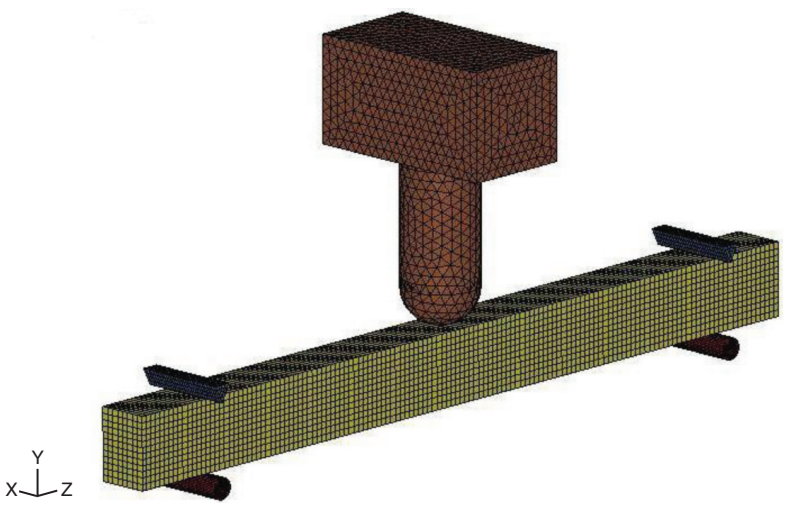

Figure 11. Typical three-dimensional FE model of RC beams

Table 4. Total number of elements and nodal points for FE model

Beam designation	Solid elements for concrete	Beam elements	Nodal points
DR3.3_2.4	22572	456	41266
DR3.3_2.4_0.12	22968	634	41900
DR3.3_2.4_0.56	24156	1258	46790
SR3.8_0.8	23760	270	42212
DR3.8_0.8_0.11	24288	818	40922
DR3.8_0.8_0.15	24640	902	52657
SR5.7_1.6	12960	270	27631
DR5.7_1.6_0.15	13248	720	28432
DR5.7_1.6_0.20	13440	776	28722

concrete nodes. The steel reinforcing bars were modeled explicitly using beam elements connected to the concrete mesh nodes. Due to this assumption of complete compatibility of strains between the concrete and steel nodes, they formed a perfect bond. The impact failure load is 70-100% higher than that of quasi-static failure load [20]. Steel deformation under impact load is limited to a region beneath the point of impact. Thus, the assumption of perfect bond in between the reinforcement and concrete was quite reasonable.

4.2. BOUNDARY CONDITION, APPLICATION OF IMPACT VELOCITY AND CONTACT ALGORITHM

Constraints were defined to the support cylinder and triangular plates, so that it could rotate about its own longitudinal axis but would not be able to translate. Triangular plates are placed 1 mm above the beam surface instead of giving the direct contact to the beam to avoid any development of restraining moment at the supports. After placing the impactor 1 mm apart from the top surface of beam at mid-span, initial velocity was defined to it to save computational time which was calculated from the free-falling formula. Constraints were defined to the impactor in such a way that it could only move in vertical downward direction. Moreover, the gravitational acceleration of impactor and self weight of beam was taken into account in this numerical simulation. Global damping (i.e., overall damping of the system) was not considered in the impact simulation here as the impact responses lasted only 30 ms. The algorithm CONTACT AUTOMATIC SURFACE TO SURFACE was used to model the contact between the support cylinder, impactor and beam. Frequent instabilities occur due to contact oscillations were stabilized by assigning a value of 30 for the viscous damping coefficient [19]. This algorithm automatically generates slave and master surfaces and uses a penalty method where nominal interface springs were used to interpenetrate between element and surfaces. The corresponding impact force due to the prescribed initial velocity to impactor was then determined by monitoring the contact forces at the concrete nodes in contact with impactor.

4.3. CONSTITUTIVE MODEL FOR CONCRETE

MAT CSCM CONCRETE (MAT 159) is commonly known as Continuous Surface Cap Model, was used to model the concrete. This model was primarily developed to simulate the deformation and damage of roadside safety concrete structures (i.e., bridge rails, safety barriers and guard rails) impacted by moving vehicles. The salient features of the models are: isotropic constitutive equations, three stress invariant yield surface with translation for pre-peak hardening, a hardening cap that expands and contracts, damage-based softening with erosion and modulus reduction, rate effects for increasing strength in high-strain rate application. Further details of the concrete model theory could be found elsewhere [21]. Moreover, the strain rate effects on concrete strength are duly considered in this model (Fig. 12). Default parameter generation option (by providing some key specifications) has been used herein instead of the traditional method where all material parameters were needed. Default parameters are provided for the concrete model based on three input specifications: the unconfined compressive strength of concrete, aggregate size and units. This option is valid for unconfined compressive strength from 20 to 58 MPa and aggregate sizes from 8 to 32 millimeters. The unconfined compressive strength affects all aspects of the fit, including stiffness, three stress invariant yield surface, hardening and damage-based softening whereas the aggregate size affects only the softening behavior of damage formulation. Mechanical properties of concrete are shown in Table 5.

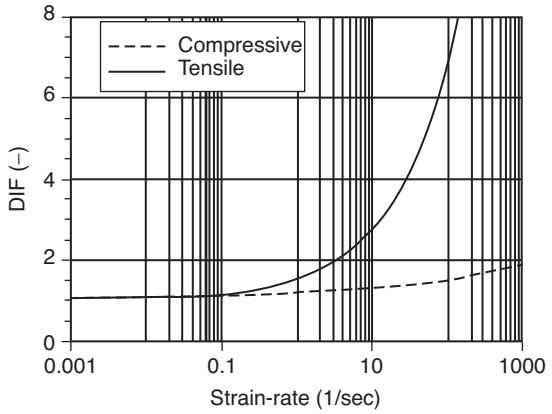

Figure 12. Approximate tensile and compressive DIF for default concrete material model (21)

Table 5. Mechanical properties of concrete

Unconfined compressive strength (MPa)	40
Elastic modulus (GPa)	29
Poisson's ratio	0.15
Bulk modulus (GPa)	12.6
Shear modulus (GPa)	13.8

Table 6. Mechanical properties of steel reinforcements

Density (kg/m^3)	7850
Yield stress (MPa)	520/310
Elastic modulus (GPa)	200
Poisson's ratio	0.3

4.4. CONSTITUTIVE MODEL FOR REINFORCING STEEL

The steel reinforcement bars (longitudinal and transverse reinforcements) within the beam are modeled as a strain sensitive uniaxial elastic-plastic material to account for its strain rate sensitivity as well as stress-strain history dependence. Material model MAT PIECEWISE LINEAR PLASTICITY (MAT 024) is used in this study to model reinforcing bars where the strain rate effects are duly considered. The expressions proposed by Malvar [18] about strain rate effects on yield and ultimate stress of steel reinforcements were employed in this study. Mechanical properties of steel reinforcement are shown in Table 6.

4.5. CONSTITUTIVE MODEL FOR IMPACTOR, SUPPORT ROLLERS AND INVERTED TRIANGULAR PLATES

MAT RIGID (MAT 020) was used from LS-DYNA [19] material library to model the impactor, support rollers and inverted triangular plates. Realistic values of Young's modulus and Poisson's ratio of the rigid material should be defined as unrealistic values may

contribute to numerical problems in contact. Young's modulus and Poisson's ratio of steel material were used for the rigid material in the numerical simulation.

4.6. VERIFICATION OF FE ANALYSIS RESULTS

To establish the reliability and accuracy of the FE model, it is essential to validate or verify the FE results with the experimental results. Time histories of midspan deflection and crack pattern (i.e. at various stages of impact loading duration) of the beams for various drop heights were used for verification. Prior to that, conservation of energy was confirmed in the simulation results. As mentioned earlier, eight node solid hexahedron elements with a single integration point were used to model concrete. Although these elements have the advantage of requiring less computational time, however, hourglass modes (i.e., nonphysical, zero-energy modes of deformation that produce zero strain and no stress) occur in these elements. LS-DYNA [19] has various algorithms for inhibiting hourglass modes. A good way to reduce hourglassing is to refine the mesh. However, to entirely eliminate this concern, the best solution is to switch the element formulation with fully- integrated or selectively reduced integration. To satisfy the conservation of energy during an impact event, the kinetic energy of impactor before impact should be equal to the sum of the current kinetic energy, the internal energy of beam and the energy loss due to friction and hourglass modes. The variation of various energies in a typical impact simulation is shown in Fig. 13. Energy loss due to friction is very small and can be neglected in above-mentioned figure. Here, hourglass energy is around 3.5% of total energy at peak impact load and around 8.5% of total energy at maximum midspan deflection (<10% as a rule-of-thumb [19]). Therefore, the low amount of hourglass energy relative to total energy in impact simulation corroborates the acceptance of analysis results. The comparison of time histories of impact load curves between test results and FE predictions is illustrated in Fig. 14. However, the discrepancy in first post peak response characteristics could be because the experimental results were affected by several factors such as the arrangement of load-cell itself and the occurrence of massive local failure at impact region. The comparison of time histories of midspan deflection curves between test results and FE predictions is displayed in Fig. 14. Successively, Fig. 15 shows the comparison of crack profiles of DR5.7_1.6_0.20 at a drop height

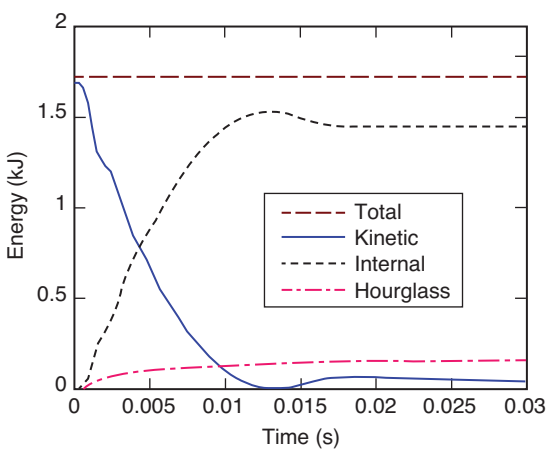

Figure 13. Variation of various energies in a typical impact simulation

(a)

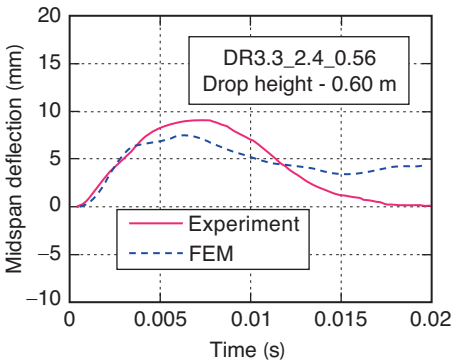

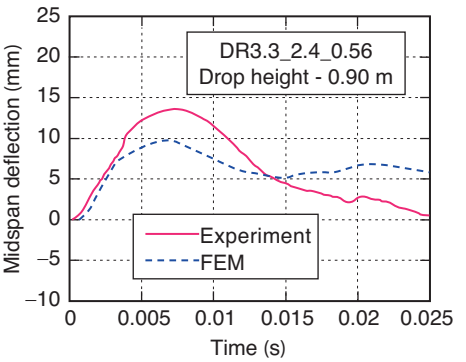

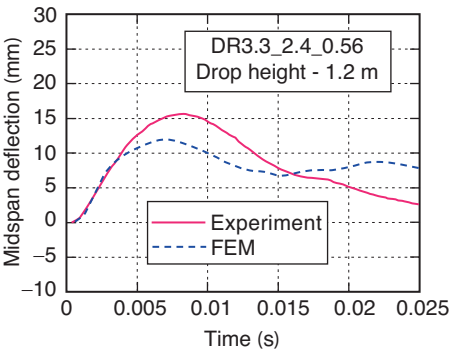

(b)

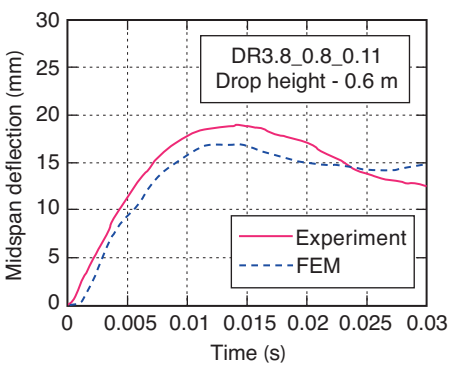

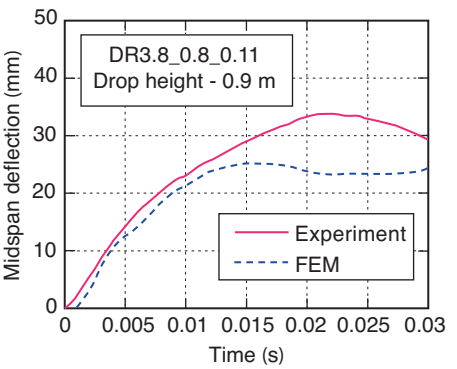

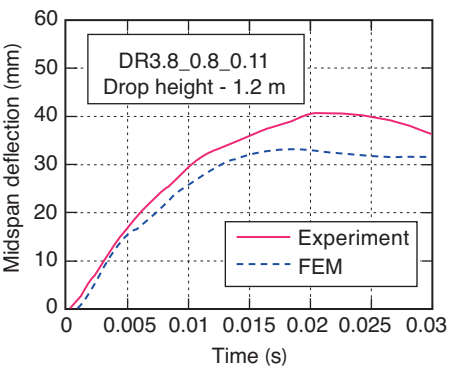

(Continued)

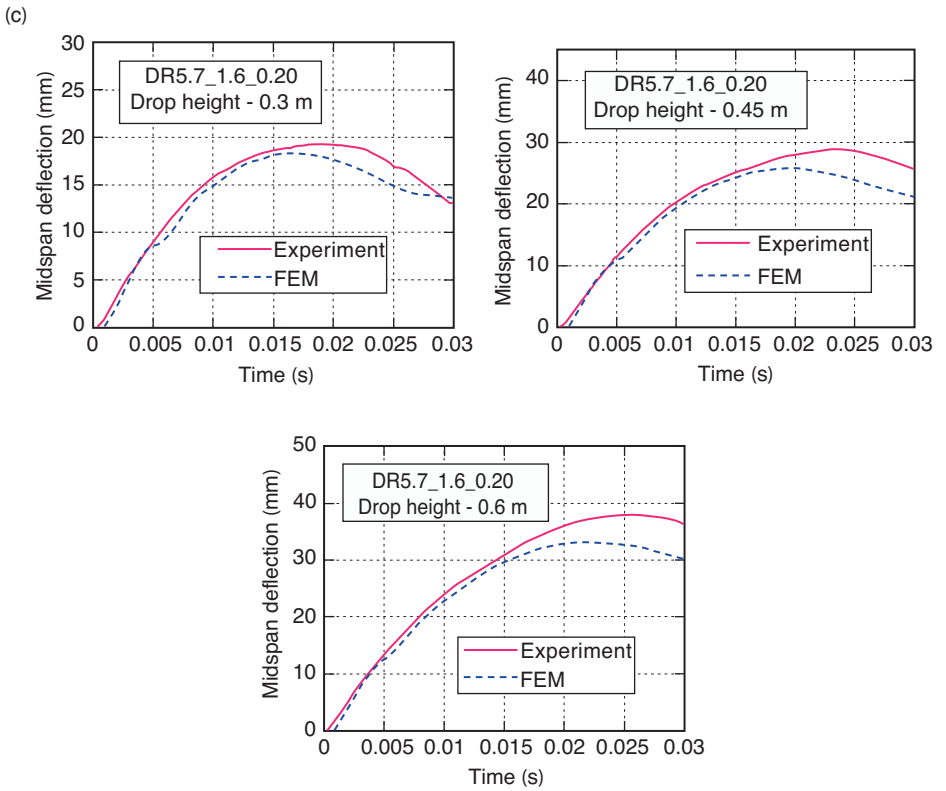

Figure 14. Comparison of time histories of midspan deflection of beams for various drop heights (a) 3.3 series; (b) 3.8 series; (c) 5.7 series

of 0.6 m. Moreover, to further validate the numerical model, the comparison of time histories of mid-span deflection curves between test results and FE predictions is shown in Fig. 16 in which RC beam specimens (i.e. S1616 and S1322) were adopted from the experimental program conducted by Fujikake et al. [4]. Table 7 which shows that percentage difference of maximum midspan deflection in between test and FEM from current study as well from Fujikake et al.[4]. Average percentage differences were around 15 and 5 respectively.

5. FE PARAMETRIC STUDY

This section presents a parametric investigation to discuss more information about the behavior of beams under varying drop heights by varying some design parameters such as mass ratio (α) i.e., ratio of the beam-mass (m_b) to impactor-mass (m_i), longitudinal reinforcement ratios (ρ_L), compressive strength of concrete (f'_c) and boundary conditions. The influence of these parameters on impact responses is summarized and discussed. The specimens considered here having clear span length and cross sections are identical to the DR beams (a/d -3.3, 3.8 and 5.7) used in the experiment.

5.1. EFFECT OF MASS RATIO (α)

Table 8 shows the variation in mass-ratios (i.e., 0.4 to 1.0) considered for each series specimens. Here the mass of the beams was kept constant; however, different mass ratios were obtained by varying the impactor-mass. For comparison, the input kinetic energy is maintained

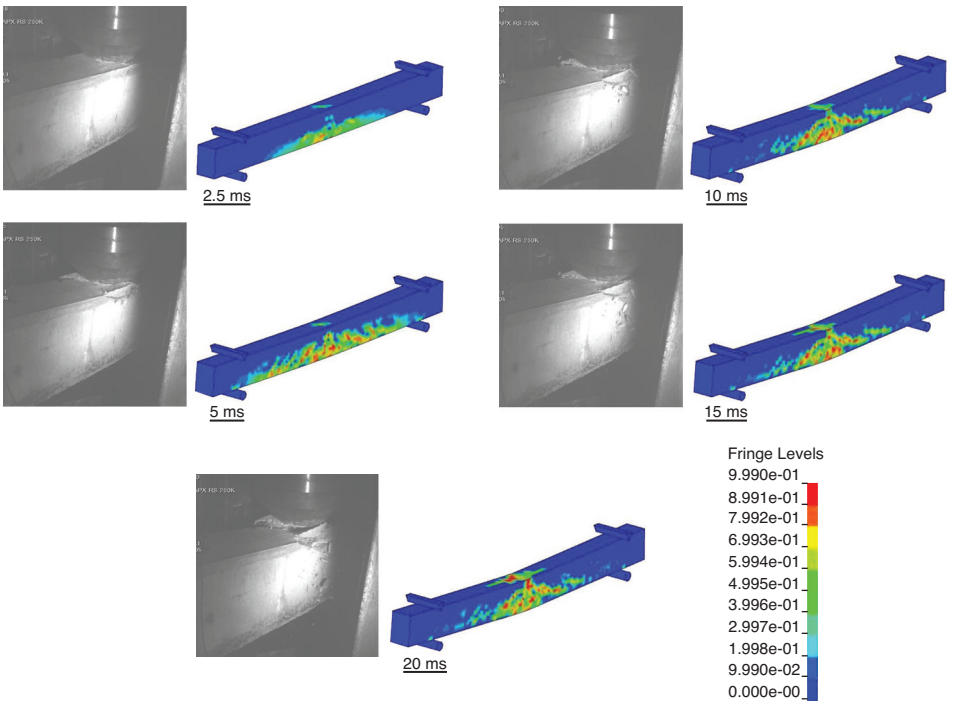

Figure 15. Comparison of crack profiles of DR5.7_1.6_0.20 at a drop height of 0.6 m

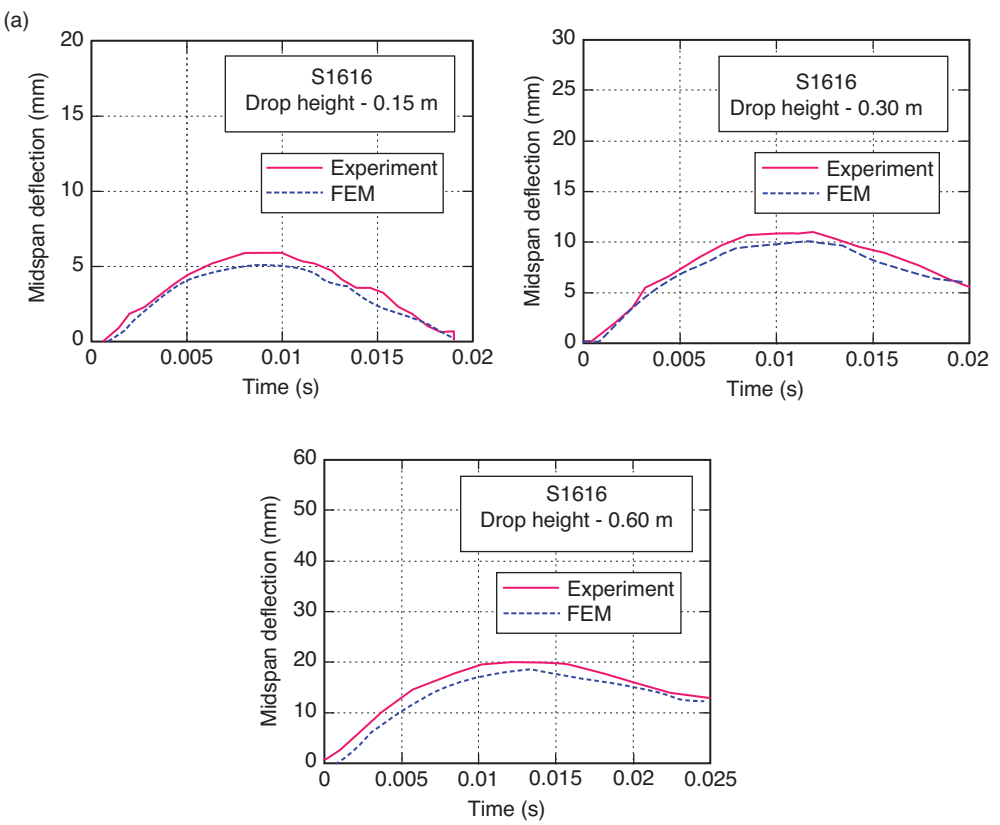

(Continued)

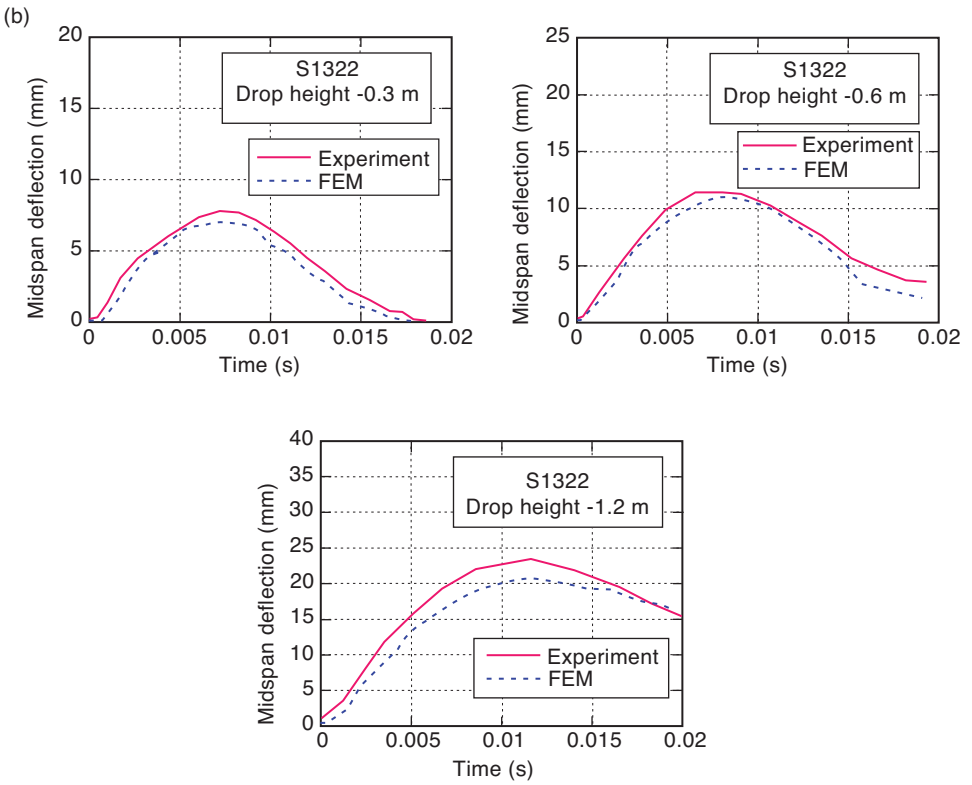

Figure 16. Comparison of time histories of mid-span deflection of beams for various drop heights (a) S1616; (b) S1322 (4)

constant whereas the impactor mass and drop-height is allowed to vary (e.g., impact energy: 2.65 kJ; impactor mass: 300, 170 and 125 kg; drop-height: 0.9, 1.59 and 2.16 m). Fig. 17 illustrates the effect of the mass ratios on maximum impact load and maximum midspan deflection of beams under varying impact energies. It is observed that under certain impact energy, maximum impact load increases and maximum midspan deflection decreases with the increment of the mass-ratios. This physically implies that under constant impact energy, impacts caused by high mass with low velocity result in smaller maximum impact load but higher maximum midspan deflection of beam and vice versa.

5.2. EFFECT OF LONGITUDINAL REINFORCEMENT RATIO (ρ_L)

The influence of longitudinal reinforcement ratio on maximum impact responses under various impact energies is presented in Fig. 18. The percentage of longitudinal reinforcement ratios (i.e., 0.8, 1.5 and 2.0%) and these ratios in terms of balanced reinforcement ratios (0.3, 0.56 and 0.75) are depicted in Table 9. Here, the mass of the impactor is considered to be 300 kg. Maximum impact load increases and maximum midspan deflection of beam decreases with the enhancement of the longitudinal reinforcement ratios. Fig. 19 presents the effect of longitudinal reinforcement ratio on failure pattern of beam under impact energy of 3.53 kJ. Severity in failure pattern

Table 7. Comparison of results in between tests and FEM

Specimens	Drop heights (m)	Impact velocity (m/s)	Maximum midspan deflection (mm)		% difference
			Test	FEM	
Current study					
	0.60	3.43	9.0	7.5	16.6
DR3.3_2.4_0.56	0.90	4.20	13.4	10.2	23.8
	1.20	4.85	15.7	12.8	18.4
	0.60	3.43	18.6	16.9	9.1
DR3.8_0.8_0.11	0.90	4.20	34.5	26.5	23.1
	1.20	4.85	41.0	34.2	16.5
	0.30	2.43	19.6	18.4	6.1
DR5.7_1.6_0.20	0.45	2.97	28.8	26.0	9.7
	0.60	3.43	39.2	33.8	13.7
				Mean	15.2
Fujikake et al. [4]					
	0.15	1.71	5.3	5	5.6
S1616	0.30	2.43	10.2	10	1.9
	0.45	2.97	20	19.7	1.5
	0.3	2.43	7.5	7	6.7
S1322	0.6	3.43	11.4	11	3.5
	1.2	4.85	23.8	21	11.7
				Mean	5.2

Table 8. Variations in mass-ratios

a/d	f_c' (MPa)	f_{Ly} (MPa)	f_{Ty} (MPa)	m_b (kg)	m_i (kg)	$\alpha = m_b/m_i$
3.3				126.0	300, 170, 125	0.42, 0.74, 1.00
3.8	40	520	310	147.5	300, 200, 150	0.49, 0.74, 1.00
5.7				78.3	150, 105, 78	0.52, 0.75, 1.00

(including diagonal and punching shear cracks) is observed with increasing amount of longitudinal reinforcements. This could be the reason behind the decrement in maximum midspan deflection when the beam contains higher amount of longitudinal reinforcements.

5.3. EFFECT OF COMPRESSIVE STRENGTH OF CONCRETE (f_c')

Beams of concrete compressive strength of 30, 40, 50 MPa was used to determine the effect of f_c' on maximum impact load and maximum midspan deflection under varying impact energies (considered mass of the impactor is 300 kg). Two case studies are depicted in Fig. 20. With the enhancement of concrete compressive strength from 30 to 50 MPa, an increasing trend in maximum impact load is observed whereas the opposite phenomenon is perceived for the case of maximum midspan deflections.

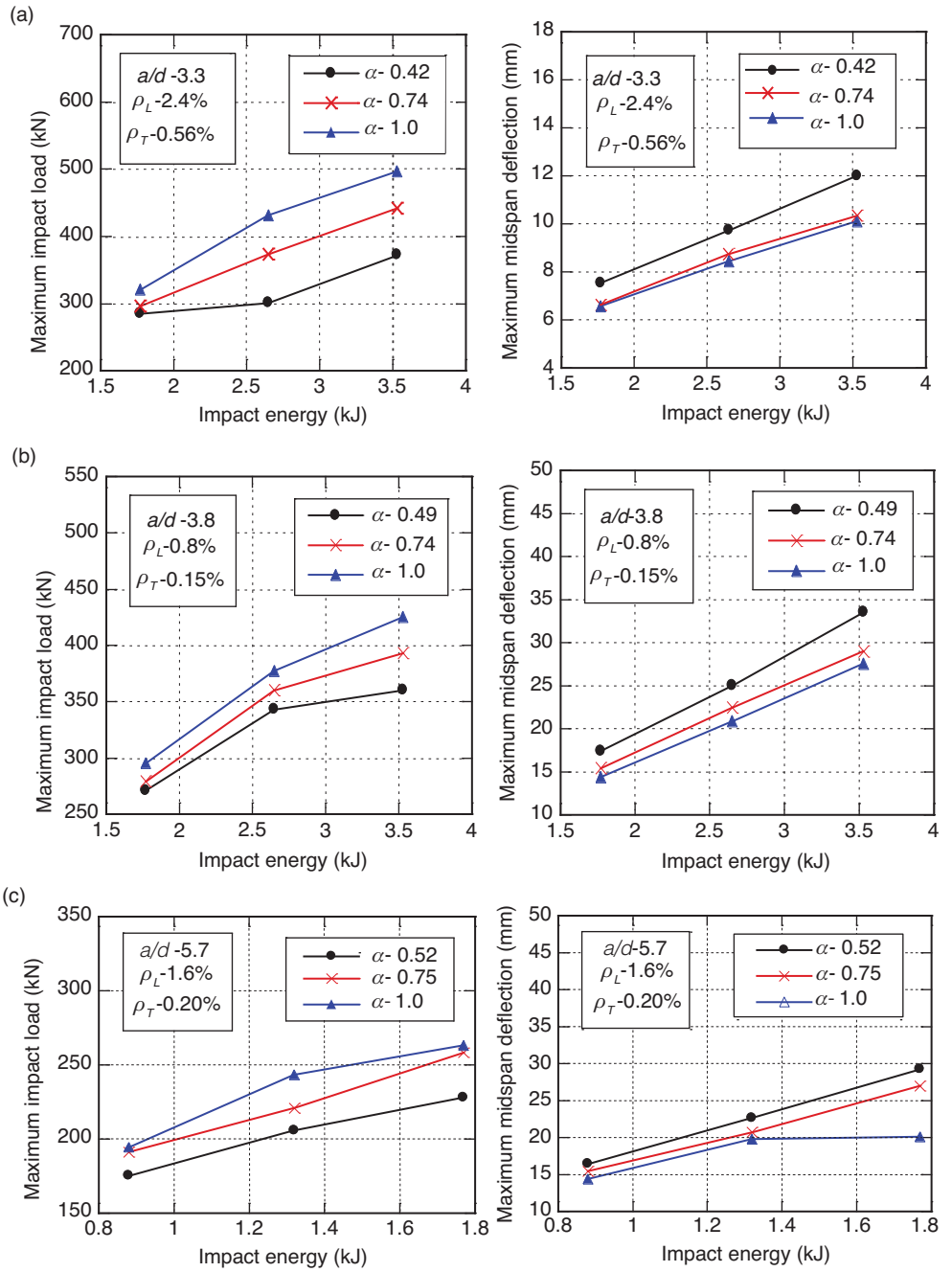

Figure 17. Effect of mass ratios on maximum impact load and maximum midspan deflection of beams (a) *a/d* -3.3; (b) *a/d* -3.8; (c) *a/d* -5.7

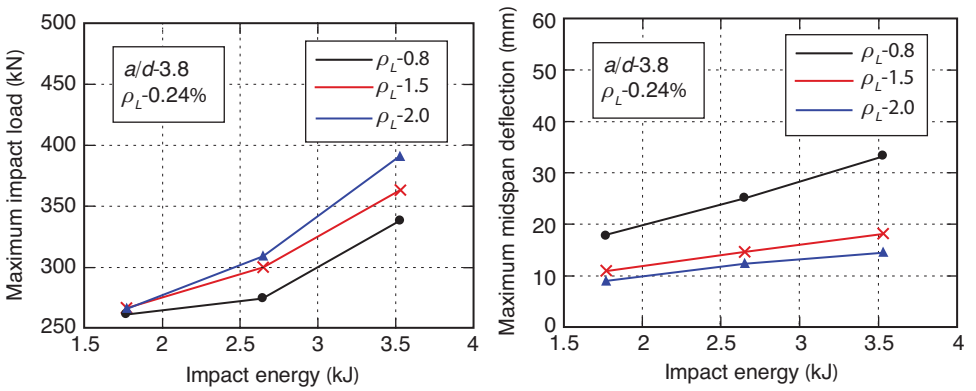

Figure 18. Effect of longitudinal reinforcement ratios on maximum impact load and maximum midspan deflection of beams

Table 9. Variations in longitudinal reinforcement ratios

a/d	f_c' (MPa)	f_{Ly} (MPa)	f_{Ty} (MPa)	ρ_b (%)	ρ_L (%)	ρ_L/ρ_b
					0.8	0.3
3.8	40	520	310	2.7	1.5	0.56
					2.0	0.75

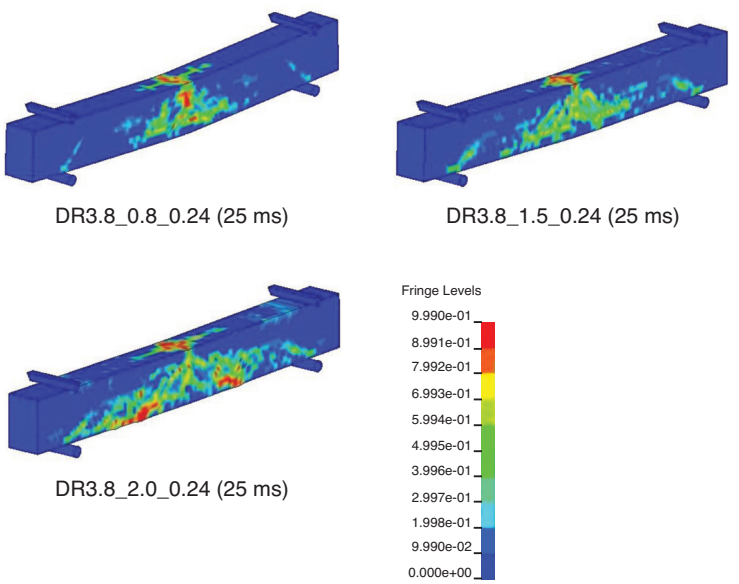

Figure 19. Effect of longitudinal reinforcement ratios on failure pattern of beam under impact energy of 3.53 kJ

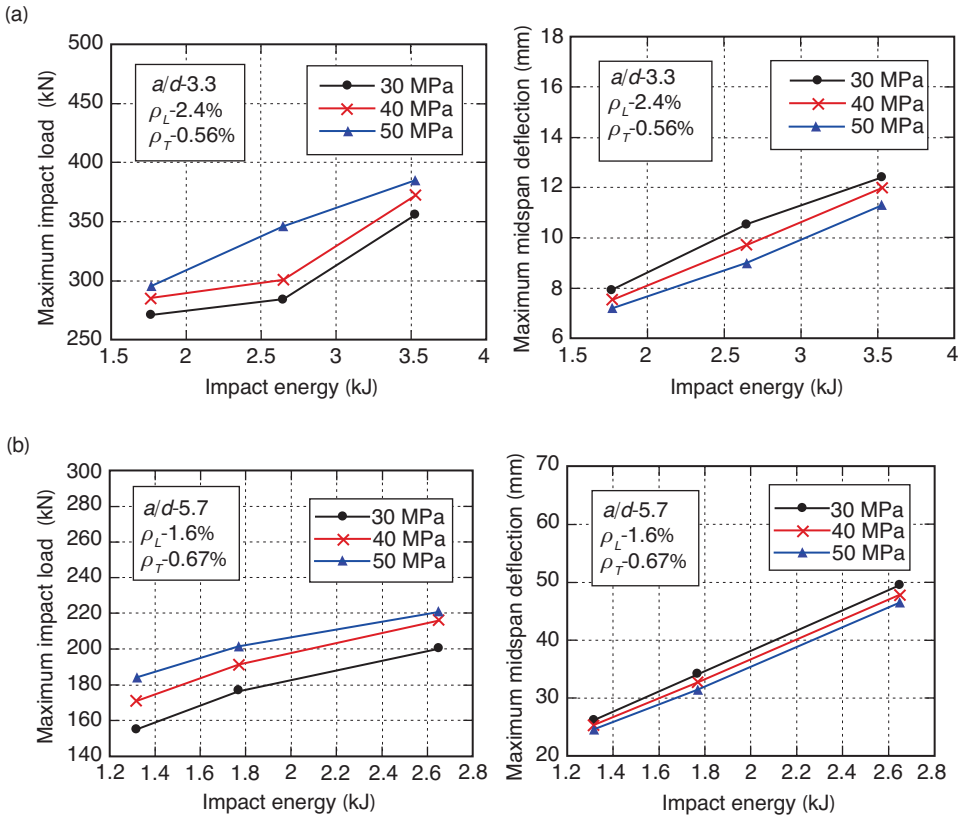

Figure 20. Effect of compressive strength of concrete on maximum impact load and maximum midspan deflection of beams (a) *a/d* -3.3; (b) *a/d* -5.7

5.4. EFFECT OF BOUNDARY CONDITIONS

To investigate the effect of boundary conditions on impact response of beam, pinned -end and fixed-end conditions are considered. Fig. 21 clearly exhibits that maximum impact load is in the higher side and maximum midspan deflection is in lower side for fixed-end beam as compared to pinned-end beam.

6. CONCLUSIONS

Based on the results presented in this paper, the following conclusions were drawn:

- Maximum midspan deflection was found to increase with the increment of drop-heights or impact velocities. Increased tendency towards shear failure of RC beam under impact loading has been mentioned by several researchers although the beam is failed in flexure under static loading. The reason would be the presence of inertia forces which is responsible for different deflected shape and subsequent higher shear to moment ratio (i.e., in higher vibration modes). Impact interface plays an important role in developing the severity of inertia forces. Harder and stiffer contact zone (i.e., when steel plate is placed in between the impactor and beam) produces more inertia forces (i.e., majority of impact energy transfer to beam through steel plate which accelerates the beam in the direction of impact force generating more inertia force) which assist

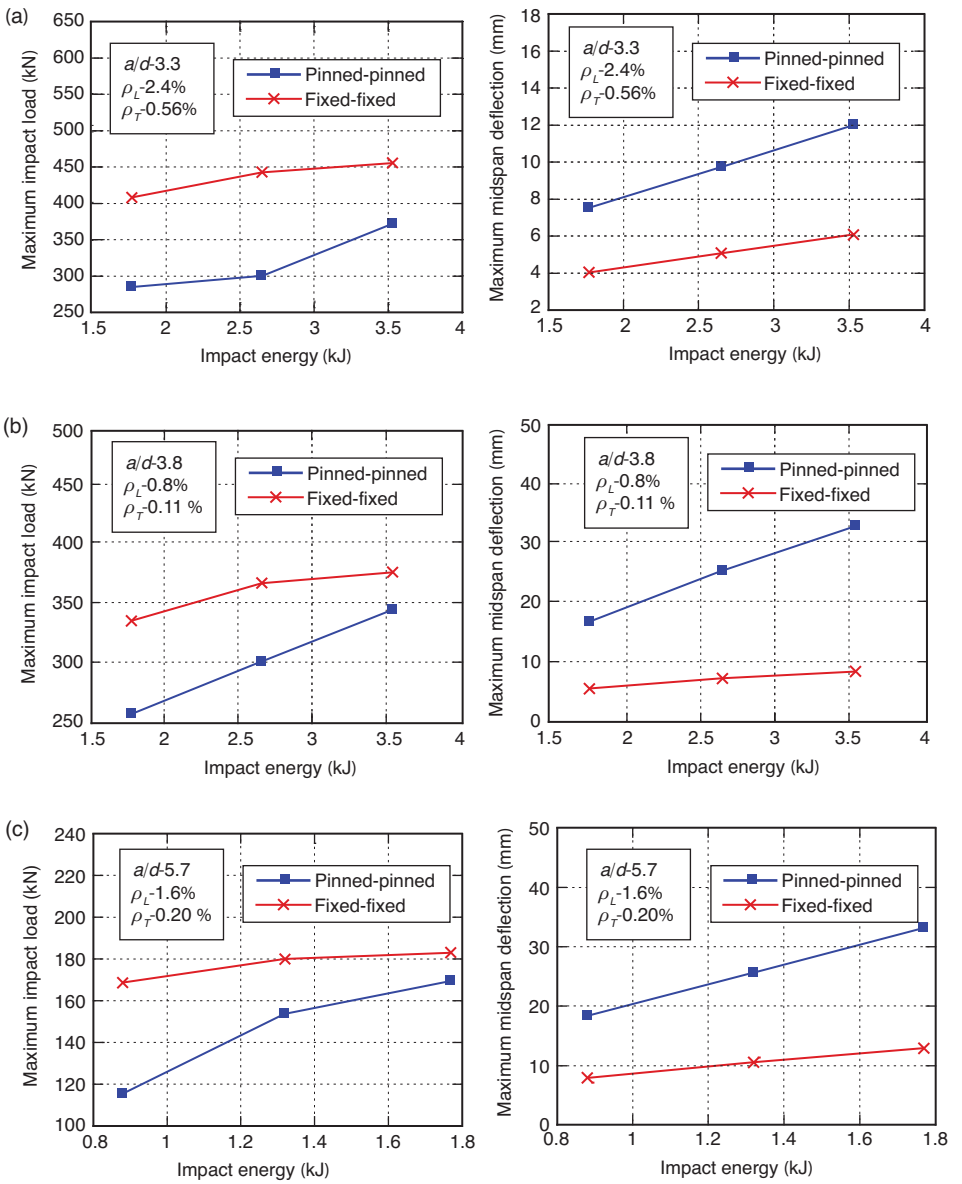

Figure 21. Effect of boundary conditions on maximum impact load and maximum midspan deflection of beams (a) *a/d* -3.3; (b) *a/d* -3.8; (c) *a/d* -5.7

beam failing in shear under impact loading. In this current test program no shear failure has been occurred in statically flexure-critical beams however with increasing the drop-heights more localized failure with extensive concrete crushing below the impactor was observed. Due to the direct contact of impactor with the beam during the impact event, majority of impact energy has been dissipated during localized crushing

of concrete in the impact region. Thus, developing less inertia force due to less energy transfer to the entire span of the beam.

- The range of maximum strain rates of longitudinal reinforcements for beams of various series under various drop-heights is provided. In general, maximum strain rates of longitudinal tensile reinforcements vary from 1 to 7 s^{-1} for the corresponding considered drop heights of 0.15 to 1.2 m (i.e. impact velocity varies from 1.72 to 4.85 m/s).
- From the numerical simulation parametric study, it is found that under constant impact energy, impacts caused by large masses with low velocity results in smaller maximum impact load but larger maximum midspan deflection of beam and vice versa. Maximum impact load increases and maximum midspan deflection of beam decreases with the enhancement of the longitudinal reinforcement ratios. With increasing longitudinal reinforcements, an increased severity of failure pattern (including diagonal and punching shear cracks) is observed. Moreover, with the enhancement of concrete compressive strength from 30 to 50 MPa, an increasing trend in maximum impact load is observed whereas the opposite phenomenon is perceived for the case of maximum midspan deflections. Finally, to assess the effect of boundary condition on impact responses, fixed-end beam has been compared with pinned-end beam. Maximum impact load is on the higher side and maximum midspan deflection is on lower side for fixed-end beam as compared to pinned-end beam.

REFERENCES

[1] Banthia, N. “Impact resistance of concrete.” PhD thesis, Department of Civil Engineering, University of British Columbia, Vancouver, B.C., Canada, 1987.

[2] Gopalaratnam, V.S., Shah, S.P., and John, R. “A modified instrumented Charpy test for cement-based composites.” *Experimental Mechanics,* 1984, 24(2), 102–111.

[3] Orozco, L.A. “Development of an Experimental Setup for Testing Scaled Versions of AASHTO Type IV Girders under Dynamic Impact Loadings.” MS thesis, The University of Texas at Austin, 2006.

[4] Fujikake, K., Li, B., and Soeun, S. “Impact Response of Reinforced Concrete Beam and Its Analytical Evaluation.” *Journal of Structural Engineering, 2009*, 135(8), 938–950.

[5] Hughes, G., and Beeby, A. W. “Investigation of the effect of impact loading on concrete beams.” *The Structural Engineer*, 60B (3), 45–52, 1982.

[6] Kishi, N., Nakano, O., Matsouka, K.G., and Ando, T. “Experimental Study on Ultimate Strength of Flexural-Failure-Type RC Beams under Impact Loading.” Transactions, SMiRT 16, Washington DC, August, 2001a.

[7] Kishi, N., Mikami, H., and Ando, T. “An applicability of the FE impact analysis on shear-failure-type RC beams with shear rebars.” Proceedings, 4th Asia-Pacific Conference on Shock and Impact Loads on Structures, 309-315, Singapore, 2001b.

[8] Kishi, N., Mikami, H., Matsuoka, K. G., and Ando, T. “Impact behavior of shear-failure type RC beams without shear rebar.” *International Journal of Impact Engineering*, 2000, 27, 955–968.

[9] Kishi, N., and Mikami, H. “Empirical Formulas for Designing Reinforced Concrete Beams under Impact Loading.” *ACI Structural Journal*, 2012, 109(4), 509–519.

[10] Chen, Y., and May, I.M. “Reinforced Concrete Members under drop-weight impacts.” *Proceedings of the ICE- Structures and Buildings*, 2009, 162(1), 45–56.

[11] Bhatti, A. Q., Kishi, N., Mikani, H., and Ando, T. “Elasto-plastic impact analysis of shear-failure-type RC beams with shear rebars.” *Materials and Design*, 2009, 30, 502–510.

[12] Tachibana, S., Masuya, H. and Nakamura, S. “Performance based design of reinforced concrete beams under impact.” *Natural Hazards and Earth System Sciences*, 2010, 10, 1069–1078.

[13] Hughes, G. and Spiers, D. “An Investigation of Beam Impact Problem.” Cement and Concrete Association, London, Technical Report No. 546, 1982.

[14] Saatci, S., and Vecchio, F. "Effects of Shear Mechanisms on Impact Behavior of Reinforced Concrete Beams." *ACI Structural Journal*, 2009, 106(1), 78–86.

[15] ACI Committee 318, "Building Code Requirements for Structural Concrete (ACI 318-08) and Commentary," American Concrete Institute, Farmington Hills, Mich., 2008.

[16] Comite Euro-International du Beton, CEB-FIP Model Code 1990, Redwood Books, Trowbridge, Wiltshire, UK, 1993.

[17] Malvar, L. J., and Ross, C. A. "Review of Strain Rate Effects for Concrete in Tension." *ACI Materials Journal*, 1998, 95(6), 735–739.

[18] Malvar, L. J. "Review of Static and Dynamic Properties of Steel Reinforcing Bars," *ACI Materials Journal*., 1998, 95(5), 609–616.

[19] LS-DYNA, Keyword User's Manual, Version 971, LST Corp, U.S.A. 2007.

[20] Weathersby, J.H. "Investigation of bond slip between concrete and steel reinforcement under dynamic loading conditions." Louisiana State University and Agricultural and Mechanical College, 2003.

[21] Murray, Y.D. (2007) "Users manual for LS-DYNA concrete material model 159." Report No. FHWA-HRT-05-062, Federal Highway Administration, Washington, DC. 2007.